Carbohydrate Polymers 79 (2010) 964–974

Contents lists available at ScienceDirect

Carbohydrate Polymers

journal homepage: www.elsevier.com/locate/carbpol

Influence of the solvent on the microencapsulation of an hydrated salt

Fabien Salaün [a,*], Eric Devaux [a], Serge Bourbigot [b], Pascal Rumeau [c]

[a] GEMTEX – ENSAIT, 9 rue de l'ermitage, BP 30329, 59100 Roubaix, France
[b] Procédés d'Élaboration des Revêtements Fonctionnels (PERF), LSPES UMR-CNRS 8008, École Nationale Supérieure de Chimie de Lille (ENSCL), BP 90108, 59652 Villeneuve d'Ascq Cedex, France
[c] IFTH, 2 rue de la recherche, 59656 Villeneuve d'Ascq, France

ARTICLE INFO

Article history:
Received 26 November 2008
Received in revised form 14 September 2009
Accepted 13 October 2009
Available online 20 October 2009

Keywords:
Microencapsulation
Phase change materials
Cellulose acetate butyrate
Hydrated salt
Thermal properties

ABSTRACT

Microparticles loaded by sodium phosphate dodecahydrate (DSP) were prepared according to the solvent evaporation–precipitation method using various organic solvent and cellulose acetate butyrate (CAB) crosslinked by methylene diisocyanate (MDI) as coating polymer. The effects of the solvent on the capsule morphology and the entrapment efficiency of water-soluble materials were investigated. The surface morphology has been investigated by SEM and it was found that the 'goodness' of the solvent, i.e. as defined by solubility parameters, strongly influences the morphology of the microparticles. Thermogravimetric analysis (TGA) and differential scanning calorimetry (DSC) were employed to investigate the thermal stability and the thermal properties of these microencapsulated phase change material. The results showed that the thermo-physical properties are strongly dependant on the core content and the synthesis conditions. Thus, the microparticles with high loading content are found suitable for thermal energy storage.

1. Introduction

Over the few past decades, preparation of uniform microparticles has received a great interest in the textile area to add new functionalities to the textile fabric (Erkan & Sariisik, 2004; Nelson, 1991, 2002). Amongst them, thermal insulation textile (Leitch & Tassinari, 2000; Pause, 1995) and more specially microencapsulation of phase change materials (PCMs) have attracted more and more attention in recent years (Cho, Kwon, & Cho, 2002; Colvin & Bryant, 1988; Fan, Zhang, Wang, Li, & Zhu, 2004; Mondal, 2008; Sarier & Onder, 2007; Zhang, Tao, Yick, & Wang, 2004). Until now, the research and development work of textile containing PCMs are essentially focused on organic compounds. The use of salt hydrates and their supercooling property are yet exploited for specialized thermal storage applications (Hirano & Saitoh, 2002; Hirano, Saitoh, Oya, & Yamazaki, 2001) and can be applied for a textile application (Talvenmaa & Meinander, 2007).

Microcapsules production can be achieved by means of physical or chemical techniques. One of them was based on solvent extraction/evaporation allowing the preparation of a wide range of microspherical and microcapsular products (Arshady, 1990). The functional performance of the microcapsules depends on the morphology, the chemical nature and the surface characteristics of the polymeric shell influenced by the process parameters. Thus, many factors such as polymer nature and concentration (El Bahri & Taverdet, 2007), emulsifiers concentration (Kistmundsdottir & Ingvarsdottir, 1994), stirring speed (Mana, Pellequer, & Lamprecht, 2007), temperature (Fundueanu et al., 2005) were selected as parameters controlling the encapsulation efficiency.

Cellulose derivatives and more specially cellulose acetate butyrate are ideally suitable for the preparation of microparticles by solvent evaporation. Fundueanu et al. (2005) have shown that the particle morphology is affected by the solvent choice and its evaporation temperature. Indeed, a high temperature allows a rapid shell formation characterized by a homogeneous and porous structure with large pores, while at low temperature a more compacted heterogeneous porous structure is obtained. Besides, the thermo-chemical and physical properties of the CAB polymeric film can be improved by crosslinking CAB with a diisocyanate via the urethane bond formation (Laskar, Vidal, Fichet, Gauthier, & Teyssié, 2004; Uda & Hijikigawa, 1988). We recently reported the development of a precipitation method intended for the entrapment of hydrated salt within CAB to form a polymeric capsule wall (Salaün, Devaux, Bourbigot, & Rumeau, 2008). In this study, we have shown that the chemical structure, the morphology and the thermal properties of the microparticles were deeply influenced by the amount of CAB and MDI introduced in the system. Thus, the optimal microparticles properties were obtained when the ratio (MDI to CAB) was found in the range of 0.4–1.

During the evaporation solvent process the polymer precipitated and encapsulated the dispersed particles upon solvent

* Corresponding author. Tel.: +33 3 20 25 64 59; fax: +33 3 20 27 25 97.
E-mail address: fabien.salaun@ensait.fr (F. Salaün).

0144-8617/$ - see front matter © 2009 Elsevier Ltd. All rights reserved.
doi:10.1016/j.carbpol.2009.10.027

evaporation. So the physico-chemical characteristics of the solvent, the interaction between polymer and solvent influence the formation and the morphology of the microparticles. Thus, the main parameter in this process is the difference between the solubility parameters of the polymer and those of the solvent and the medium (Moldenhauer & Nairn, 1992). The main objective of this study was to design solvent systems on the basis of the comparison of the solubility parameters of the solvent, polymer and aqueous active substance phases, which produce microparticles with optimum properties. The solvent solubilizing CAB and the solvent of the continuous phase were selected on the basis of the Hansen solubility parameters (Hansen, 1967, 1969). The influence of these solvents on the morphology, loading content and thermal properties was also investigated.

2. Experimental

2.1. Materials

Cellulose acetate butyrate (CAB) (13.5 wt.% acetyl and 38 wt.% butyryl content, average Mn ca. 30,000) was purchased from Aldrich. The degree of substitution of butyryl was 1.7, of acetyl 1.05 and of hydroxyl 0.25. Diphenyl methylene diisocyanate (MDI) (Suprasec 2030, Hüntsman ICI; blend of MDI isomers, 4,4′-diphenyl methylene diisocyanate principally) was used to react with CAB. Sodium phosphate dodecahydrate, $Na_2HPO_4{\cdot}12H_2O$ (DSP) was employed as core material. Non-ionic surfactant, Span® 85 (sorbitan trioleate) was purchased from Aldrich, and used as emulsifier. Acetone, toluene, carbon tetrachloride and chloroform used were reagent grade.

2.2. Preparation of microparticles

Microencapsulation by solvent evaporation basically consists of four steps (Freitas, Merkle, & Gander, 2005). The active substance is dispersed in an organic solvent containing the polymeric wall. Next, this phase is emulsified in an immiscible polymer non-solvent continuous phase. Polymer coating around the active substance particles occurs as a result of portioning of the polymer solvent from the dispersed phase to the continuous phase, accompanied by solvent evaporation. Finally, solid particles are recovered after washing, filtration and drying. In our study, the experimental

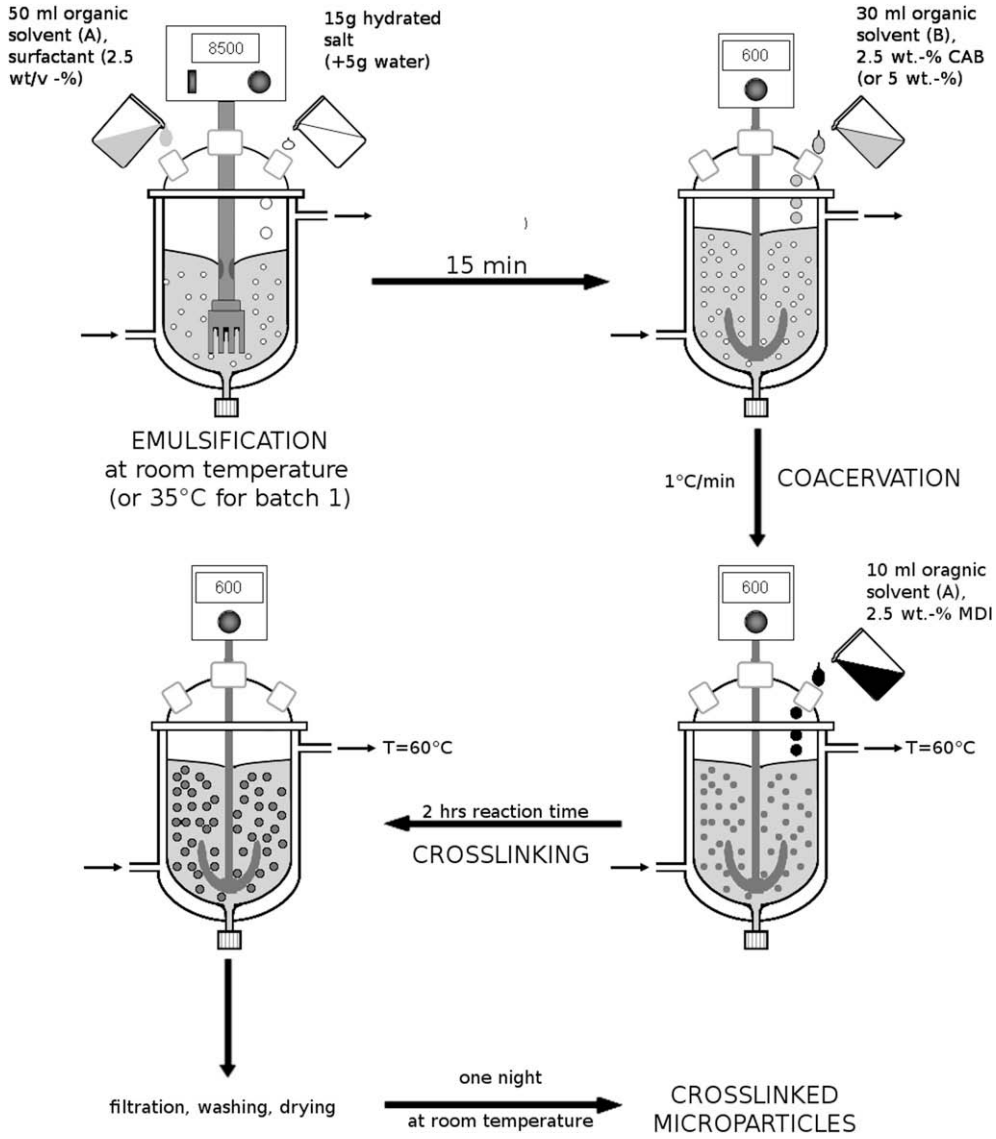

Fig. 1. Schematic representation of the various stages of the microencapsulation process by the solvent evaporation–precipitation method.

procedure is derived from an interfacial polymerization used for the polyurethane microcapsule preparation coupled with a solvent evaporation.

The preparation of the microparticles was carried out according to the following method. An aqueous phase containing 15 g of hydrated salt was emulsified at a stirring rate of 8500 rpm with a homogenizer (ultra turrax®, Ika, Germany) at room temperature (or at 35 °C for batch 1) in 50 ml of an organic phase. The organic phase was prepared by dissolving the surfactant in a non-volatile solvent (carbon tetrachloride or toluene). After 15 min, when the expected droplet size of the emulsion was reached, a solution containing 2.5 wt.% (or 5 wt.%) of CAB previously solubilized in 30 ml of a volatile solvent (acetone or chloroform) is added. The mixture was stirred continuously using a blade stirrer at a lower speed (600 rpm) under ambient pressure and the temperature was increased at 1 °C/min until 60 °C to allow the progressive evaporation of volatile solvent. The complete crosslinking of the microparticles was carried on by a drop-wise addition of a solution containing 2.5 wt.% of MDI in 10 ml of toluene (or carbon tetrachloride), until the polymerization was completed (2 h). The resultant microparticles were recovered by filtration and washed with toluene to remove remaining MDI and dried at room temperature for one night. A schematic description of the various stages of the microencapsulation process is given in Fig. 1.

2.3. Analysis of the microparticles

The microscopic aspects of the particles were observed by optical microscopy (Axioskos Zeiss) equipped with a camera (IVC 800 12S). The surface morphology of the microparticles and their compositional analysis were observed with the help of a scanning electron microscopy (Philips XL30 ESEM/EDAX-SAPPHIRE) at an accelerated voltage of 12 kV.

The thermal behavior of the particles was recorded using a TA instrument type DSC 2920 piloted on PC with TA Advantage control software. Indium was used as standard for temperature calibration and the analysis was made under a constant stream of nitrogen (50 ml/min). Samples were placed in aluminum pans which were hermetically sealed before being placed on the calorimeter thermocouples. The sample space was purged with nitrogen at a constant flow (50 ml/min) during the experiments. Transition temperatures and enthalpies were obtained from a least four independent experiments on (10.0±)-mg samples with a scanning speed of 2 K min^{-1}. The temperature ranges presented in this work were from −30 to 80 °C (batch 2), −30 to 100 °C (batches 3, 4 and 6) and −30 to 60 °C for batch 5. The thermal program used for batch 2 (isothermally held at −30 °C for 3 min, ramp at 2 °C/min to 80 °C, isothermally held at 80 °C for 3 min, ramp at 2 °C/min to −30 °C, isothermally held at −30 °C for 3 min, ramp at 2 °C/min to 80 °C, isothermally held at 80 °C for 3 min, ramp at 2 °C/min to −30 °C) was used to show the crystallization behavior of the hydrated salt and specially its incongruent melting and the dehydration phenomenon occurring during this test.

Thermogravimetric analyser (TA Instruments type TGA 2950) was used to record the thermograms in the temperature range from 30 to 800 °C with a heating rate of 10 K min^{-1} in a flow of nitrogen gas at 60 ml min^{-1}. The salt content was calculated as the ratio of the residual weight at 600 °C divided by the residual weight at 150 °C corresponding to the weight of the fully dehydrated salt and the microparticles containing the fully dehydrated salt, respectively.

The encapsulation yield was calculated as the ratio of the mass of microparticles shell (after correction of salt content determined by thermogravimetric analysis (TGA), Table 1) obtained at the end of the process and the mass of initial substances added including CAB and MDI. To remove the effects of residual moisture and water content, the TGA spectra were normalized to 100 wt.% at 140 °C.

3. Results and discussion

3.1. Solvent selection according to CAB solvency

3.1.1. Empirical approach

The prediction of the solubility of a polymer in an organic liquid was proposed by Hansen (Hansen, 1967). The Hansen solubility parameters consist of three components, with a dispersion term δ_d, a polar term δ_p, and a hydrogen-bonding term δ_h, which together make up the total solubility parameter δ_t, and their relationship can be expressed as in Eqs. (1) and (2):

$$\delta_t^2 = \delta_d^2 + \delta_p^2 + \delta_h^2 \quad (1)$$

$$\delta_t = \sqrt{\frac{E}{V}} \quad (2)$$

where, E is the vaporization energy of the compound, and V is the molar volume of a compound. Furthermore, according to Hansen, the region of good solubility can be characterized by the distance

Table 1
Preparation of microparticles. Influence of the solvent choice on microparticle characteristics: Yield, salt content, and appearance of microcapartciles.

No. of batch	Organic solvent		Yield[a] (%)	Salt content[b] (wt.%)	T_g[c] (°C)	State and surface, appearance of microparticles[d]	Note
	Continuous phase (solvent B)	Dispersed phase (solvent A)					
1	Carbon tetrachloride	Acetone	52.3	74.2	115	Few particles, deformed and some broken particles, aggregation, smooth surface	15 g of DSP 2.5%-wt of CAB
2	Carbon tetrachloride	Acetone	52.0	57.9	124	Irregular shape, large distribution, aggregation, rough surface	15 g of DSP + 5 g H_2O 2.5%-wt of CAB
3	Carbon tetrachloride	Chloroform	92.0	77.1	127	Almost spherical shape, narrow size distribution rough surface	15 g of DSP + 5 g H_2O 2.5%-wt of CAB
4	Toluene	Chloroform	41.6	23.8	131	Irregular shape, large distribution, aggregation, very rough surface	15 g of DSP + 5 g H_2O 2.5%-wt of CAB
5	Toluene	Chloroform	68.4	49	124	Almost spherical shape, narrow size distribution, aggregation, smooth surface	15 g of DSP + 5 g H_2O 5%-wt of CAB
6	Toluene	Toluene	33.1	77.8	117	Pelicules, irregular shape	15 g of DSP + 5 g H_2O 2.5%-wt of CAB

[a] The yield is identical to monomer conversion.
[b] Determined by TGA.
[c] Determined by DSC.
[d] Observed by SEM.

between solvent and polymer and defined as a sphere in the three-dimensional space of the solubility parameters. The corresponding interaction radius for solvent i and polymer j is therefore given by Eq. (3):

$$R_{ij} = [4(\delta_{d,i} - \delta_{d,j})^2 + (\delta_{p,i} - \delta_{p,j})^2 + (\delta_{h,i} - \delta_{h,j})^2]^{\frac{1}{2}} \quad (3)$$

This means that a polymer is probably soluble in a solvent if the Hansen parameters for the solvent lie within the solubility sphere for the polymer. In order to predict the solubility, the distance R_{ij} must be less than the radius of interaction R_j of the polymer. A simple composite affinity parameter, the RED (Relative Energy Difference) number, has been defined according to Eq. (4):

$$RED = \frac{R_{ij}}{R_j} \quad (4)$$

3.1.2. Calculation of Hansen parameters for CAB

The values of δ_d, δ_p, δ_h were estimated based on the chemical structure of the polymer unit with the approaches published by van Krevelen & Hoftyzer (1990) and Hoy (1989). As the results of the two methods for estimation of Hansen solubility parameters are of the same order of accuracy, the average results were taken.

The interaction radius, R_j, for CAB was chosen to include as many solvents in the solubility sphere and partial solvents on the surface of the soluble region, and, exclude as many non-solvents as possible. Twenty-nine solvents were tested to evaluate solubilization of cellulose acetate butyrate and are tabulated in Table 2. As a result, most of solvents dissolving CAB are included in the spherical region which is expressed by Eq. (3) with R_j = 9, δ_d = 17.7, δ_p = 6.6 and δ_h = 8.9 $MPa^{1/2}$ (Fig. 2).

3.2. Formation of microparticles by the solvent evaporation–precipitation method

The encapsulation process was achieved as a liquid phase separation conducted in an organic phase: (1) the core material was well dispersed into an organic solvent (A); (2) the wall material (CAB) was dissolved in solvent (B) and added to the previous solution; and (3) solvent (B), called a coacervation agent, which dissolves solvent (A) in order to desolvate partially the wall material but not completely, and a crosslinker (MDI) are added to the dispersion. The polyurethane shell is formed by reaction of the hydroxyl groups of CAB with isocyanate groups of MDI at the interface. Interfacial polymerization occurs rapidly at 60 °C. Furthermore, MDI monomers can be hydrolyzed slowly at the interface to form amines which react with MDI monomer to form a part of the shell. In this way, DSP particles are gradually coated by the partial desolvated macromolecular aggregates or the formed coacervates. If the rate of coacervate addition is too fast, polymer precipitation easily occurs (Tianyong, Xuening, Jian, & Chunlong, 1999). During this encapsulation method, the polymer precipitated and encapsulated the dispersed particles upon solvent (B) evaporation. So the physico-chemical characteristics of the solvent, the interaction between polymer and solvent would influence the formation of the microparticles.

In order to validate the above criteria as the selection guides to appropriate solvents, four solvents were selected from candidates (solvent A) and non-candidates (solvent B), and used to produce microparticles: acetone and chloroform from candidates; toluene and carbon tetrachloride were chosen to initiate the polymer coacervation and precipitation. Six different batches of microparticles were prepared using three couple of organic solvents. Two of these batches (1 and 2) were prepared to study the effect of water in the dispersed phase on the characteristics of the microparticles in

Table 2
Solubility parameters and relative energy difference, RED, of various solvents for CAB.

Solvent	δ[a] ($MPa^{½}$)	δ_d[a] ($MPa^{½}$)	δ_p[a] ($MPa^{½}$)	δ_h[a] ($MPa^{½}$)	Solubility	RED
Diethyl ether	15.6	14.5	2.9	5.1	Non-solvent	0.924
Dichloromethane	20.2	18.2	6.3	6.1	Solvent	0.332
Acetone	19.9	15.5	10.4	7.0	Solvent	0.680
Chloroform	18.9	17.8	3.1	5.7	Solvent	0.527
Methanol	29.6	15.1	12.3	22.3	Non-solvent	1.718
Tetrahydrofuran	19.5	16.8	5.7	8.0	Solvent	0.245
n-Hexane	14.9	14.9	0.0	0.0	Non-solvent	1.379
Carbon tetrachloride	17.8	17.8	0.0	0.6	Partial solvent	1.178
Ethyl acetate	18.2	15.8	5.3	7.2	Solvent	0.485
Ethanol	26.5	15.8	8.8	19.4	Non-solvent	1.265
2-Butanone	19.1	16.0	9.0	5.1	Solvent	0.626
Cyclohexane	16.8	16.8	0.0	0.2	Non-solvent	1.230
Dichloroethane	20.0	17.4	5.3	4.1	Solvent	0.557
Acetonitrile	24.4	15.3	18.0	6.1	Solvent	1.409
Water	47.8	15.6	16.0	42.3	Non-solvent	3.883
Nitromethane	25.1	15.8	18.8	5.1	Solvent	1.481
Toluene	18.2	18.0	1.4	2.0	Partial solvent	0.962
Isobutyl acetate	16.8	15.1	3.7	6.3	Solvent	0.722
n-Butanol	22.2	15.8	5.7	14.5	Non-solvent	0.759
Butyl acetate	17.4	15.8	3.7	6.3	Solvent	0.605
Xylene	18.1	17.8	1.0	3.1	Partial solvent	0.896
Propanoic acid	19.9	14.7	5.3	12.4	Solvent	0.785
N,*N*-Dimethylformamide	24.9	17.4	13.7	11.3	Solvent	0.835
Cyclohexanone	19.6	17.8	6.3	5.1	Solvent	0.424
Benzaldehyde	21.4	19.4	7.4	5.3	Solvent	0.557
Dimethyl sulfoxide	26.7	18.4	16.4	10.2	Solvent	1.109
Ethylene glycol	33.0	17.0	11.0	26.0	Non-solvent	1.968
Benzylalcohol	23.8	18.4	6.3	13.7	Solvent	0.557
Nitrobenzene	22.2	20.0	8.6	4.1	Solvent	0.771

[a] δ is the Hildebrand solubility parameter, and δ_p, δ_d and δ_h are the Hansen partial solubility parameters [$MPa^{1/2}$] representing the polar, dispersive and hydrogen-bonding cohesive forces.

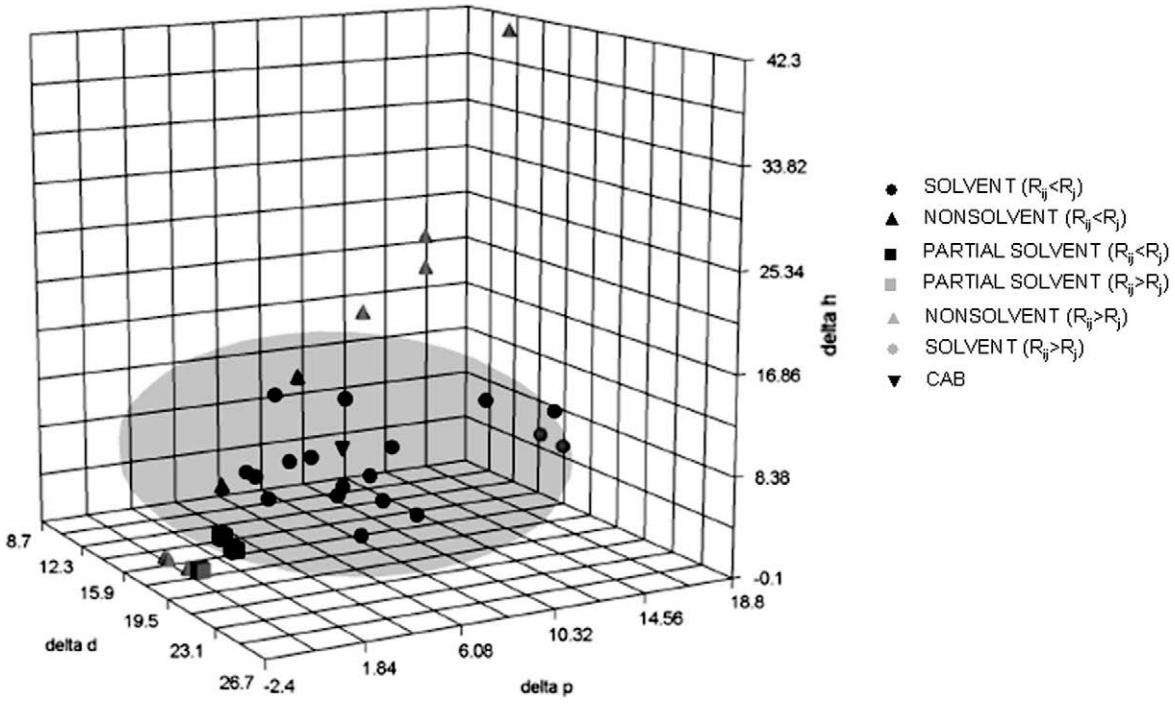

Fig. 2. 3-Dimensional plot of the cellulose acetate butyrate sphere of surface affinity and the tested solvents used.

presence of carbon tetrachloride. The influence of the organic solvents solubilizing CAB was performed from the batches 2 and 3. The batches 4 and 5 were prepared to study the effect of a change in the DSP/polymer ratio on the characteristics of the microparticles in the presence of toluene. The batch 6 was used for comparison.

Figs. 3 and 4 show the SEM pictures of the microparticles prepared in the presence of carbon tetrachloride (batches 1, 2 and 3) and toluene (batches 4, 5 and 6), respectively. From these figures, it seems that the morphology of the microparticles greatly depended on the solvent system. In the case of carbon tetrachloride as continuous phase, the only successful batch was the one that contained chloroform (batch 3). The use of acetone results in dehydration of DSP and therefore in incompletely covered particles. Furthermore, the increase of water content in the dispersed phase (batch 2) allows to obtain a more uniform shell but also aggregated particles (Fig. 3). Spherical particles with relatively uniform size (mean diameter about 3 μm) were observed for the substitution of acetone for chloroform in the batch 3. However, even with this batch, the amount of aggregated particles remains relatively high. This phenomenon can be induced by the tendency of the microparticles to aggregate when the volume of the inner phase decreases

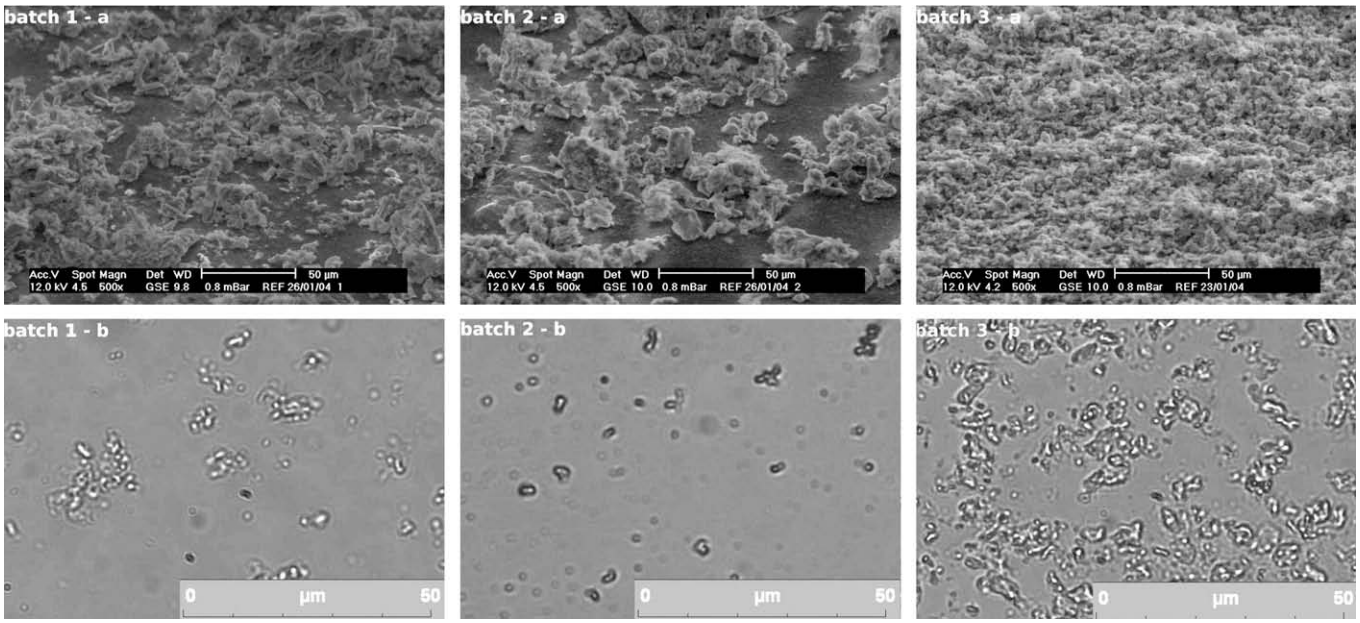

Fig. 3. Scanning electron (a) and optical (b) micrographs and of CAB/MDI microparticles from batch nos. 1, 2 and 3 at a magnification of 500 and 64 times, respectively.

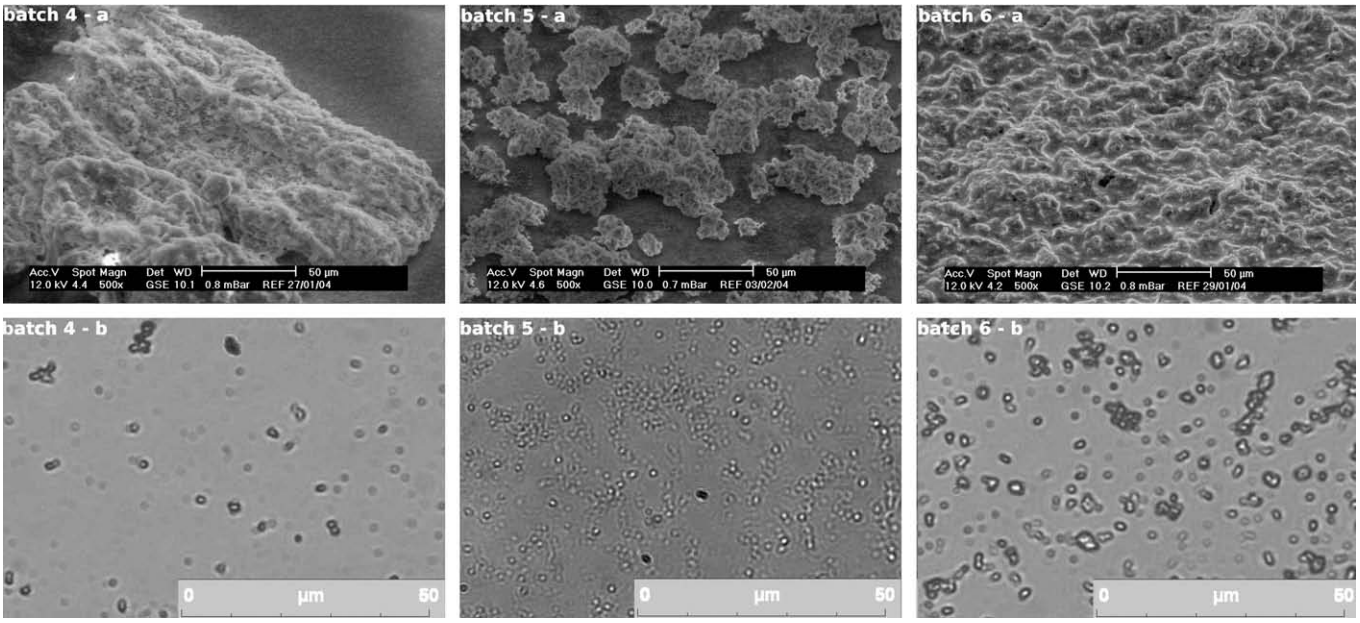

Fig. 4. Scanning electron (a) and optical (b) micrographs of CAB/MDI microparticles from batch nos. 4, 5, and 6 at a magnification of 500 and 64 times, respectively.

during the solvent removal as compared with the continuous phase. The decreasing of the dispersed phase volume increases the number of collisions of the particles and therefore the aggregation. Furthermore, the CAB precipitates slowly due to slow removal of chloroform allowing the formation of smoother shell. These particles were clearly separated from each other, and with this batch, the efficiency of particle formation was high, and typically over 90% of the wall material in the batch formed round particles.

The substitution of carbon tetrachloride for toluene modifies the rate of polymer precipitation at the interface and therefore the surface appearance of the microparticles (Fig. 4). Toluene is a partial solvent for CAB and therefore decreases the rate of coacervation. Nevertheless, the density mismatch causes severe sedimentation problem during the process. Closed examinations (Fig. 5) revealed that the particles were formed as a sticky aggregate of smaller polymer droplets rather than a continuous film. Since the wall material was formed by interfacial polymerization with the adding of MDI, the formation of aggregated structure is due to a limited solubility of oligomer in solvent. Moreover, subsequent reaction with hydroxyl groups of CAB from other outer shell particles and entanglement to form solid particles which then aggregate at the interface promote this phenomenon. Yield was slightly higher (68.4%) if the concentration of the CAB solution was 5% (batch 5) rather than 2.5% (batch 4) which was due to the increase of the viscosity. The viscosity of the CAB solution also greatly affected the formation of aggregates and the particle size distribution. Thanks to the stabilizing effect of highly viscous solution, sedimentation effect was reduced allowing the formation of smoother surface. The amount of aggregated polymer was decreased markedly, but the formed particles still seemed to be partially adhered to each other. Use of toluene as solvents A and B (batch 6) did not produce microparticles but only a film containing dispersed DSP particles (Fig. 4). Although the solubility of CAB in toluene is low, there might have been some polymer–toluene interactions that did not promote the precipitation of the CAB optimally. Therefore, the encapsulation yield obtained was slightly lower.

Figs. 3 and 4 depict also OM images of the microparticles produced with various organic solvents and the aggregation structure of the microparticles disappears when they are suspended in solution. Spherical and mono-sized particles were ascertained from the microscopic images. The obtained microparticles are better defined when toluene was used as continuous phase rather than carbon tetrachloride. Furthermore, the use of chloroform as non-solvent with carbon tetrachloride results in the formation of tiny droplets of hydrated salt dispersed in the polymeric matrix. For optical analysis of batch 6, microparticles were dispersed in toluene (before water) to avoid film formation (see in SEM micrograph in Fig. 4), toluene swells and partially solubilizes CAB which does

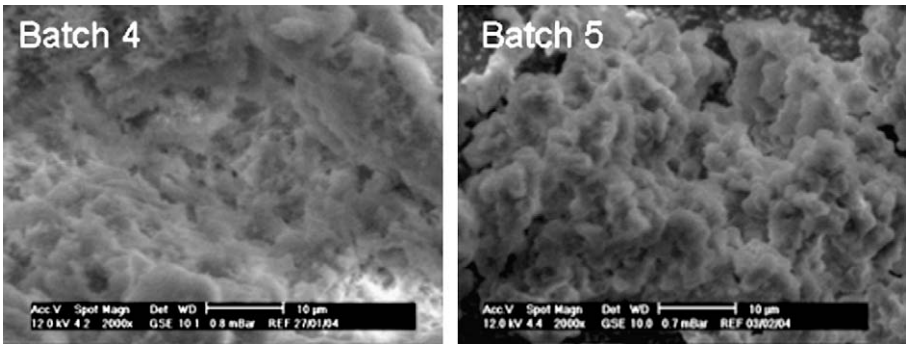

Fig. 5. Scanning electron micrographs of CAB/MDI microparticles from batch nos. 4 and 5 at a magnification of 2000 times.

not react with MDI, and as a result, mono-sized particle are observed.

3.3. Thermal properties of the microparticles

The permeability properties of the microparticles are also governed by the thermal properties of microparticles wall membranes. T_g recorded changes can be related to some physico-chemical modifications occurring in the polymer during solvent evaporation process (Torres, Boado, Blanco, & Vila-Jato, 1998) e.g. it is closely related to the film formation. In this study, a second run was necessary to clearly distinguish the T_g of microparticles. The T_g of various microparticles is lower than the one of the raw CAB (133 °C). Thus, the crosslinking reaction between CAB and MDI causes a decrease in the T_g value due a decrease in the extent of hydrogen bonding. Besides, the glass transition temperature of capsule wall was found to decrease with increasing the core content material, indicating a plasticizing effect of DSP. Significant differences were observed when formulations made using acetone were compared with those made from chloroform and when carbon tetrachloride was substituted by toluene. These changes recorded could be related to some physico-chemical changes and to the rate of precipitation occurring in the microparticle shell during solvent evaporation. As seen in the previous part, the substitution of acetone for chloroform decreases the rate of polymer precipitation and results in higher encapsulation yield. Therefore, CAB network with higher crosslink density is obtained since the $NCO/OH_{accessibles}$ molar ratio increases and consequently higher T_g value. The use of toluene, a partial solvent, as solvent B rather than carbon tetrachloride, a non-solvent results in an increase of T_g value whereas the salt content decreases. Toluene is effective for swelling CAB allowing the salt diffusion through the polymer membrane and therefore promotes the reaction between MDI and water molecules to the detriment of the crosslink reaction between CAB and MDI. Then, these oligomers could react with a small amount of CAB to form a crosslinked network explaining the higher T_g value of the batch 4. The increase of CAB concentration (batch no. 5) and the substitution of solvent A for toluene influence the viscosity and the solidification rate of the polymer phase. The increase of polymer solution viscosity delays salt diffusion through the polymer membrane and promotes the precipitation of a highly concentrated polymer solution. Therefore, once the polymer is solidified, the encapsulated salt does not easily escape from the shell and can act as plasticizer agent, e.g. T_g value decreases.

3.4. Thermal stability

The thermal degradation of DSP has been already reported elsewhere (Ghule, Bhonghale, & Chang, 2003). The thermal dehydration and condensation processes of disodium hydrogen dodecahydrate show a loss of 59.3% weight in the entire dehydration process contributing to the loss of 12 water molecules between 30 and 84 °C. Furthermore, in the temperature range from 246 to 345 °C, Na_4PO_7 formation resulting from the condensation process was observed. Between 345 and 600 °C no weight loss was observed. Besides, the thermal degradation of CAB occurs in two consecutive stages, with the first being the main one. The first was in the range of 250–370 °C with a weight loss of 86.4% and it represented the main thermal degradation of the cellulose acetate chains. The char formed from the first step of the degradation is oxidized during the second stage of decomposition, in the range of 370–520 °C with a weight loss of 13.6% (Table 3).

The TG and DTG curves of various microparticles are shown in Figs. 6 and 7. The residual weight of each sample is related to the difference of chemical structure and the DSP amount contained in the core. The thermal degradation of CAB/MDI microparticles occur in four main steps. The weight loss starts at 100 °C with evolving water. The weight loss of microparticles at temperatures between 200 and 420 °C (steps II and III) may be attributed to the decomposition of CAB/MDI network. Thus, from 280 °C, the degradation and the depolymerization of polyurethane polymer and oligomers were observed. Most of the reactions implied in the degradation mechanism lead to the formation of crosslinked compounds with urea groups. This step was followed by a recombination in urea oligomers, which were degraded at higher temperature, between 420 and 600 °C (step IV). While no change in onset temperature of degradation ($T_{10wt.\%}$, 10% weight loss temperature) of samples from batch nos. 1, 2, 3 and 4 is observed, it is decreased by about 100 °C in the case of sample no. 5 and it is increased by about 10 °C in the case of sample no. 6. It can be explained by the fact that the surface of sample no. 6 is smoother, which results in the decrease of the diffusion rate of the core material. Whereas, the weight losses of the first stage for the samples no. 5 is probably due to the elimination of the adsorption water of the microparticles and the hydration water of the hydroxyl groups of CAB. Owing to the high thermal decomposition temperature of the CAB/MDI crosslinked shell, the weight loss rates of microparticles (batch nos. 1, 2, 3, 5 and 6) decrease between 280 and 320 °C. As a result, the slopes of TGA curves of microparticles become smaller. As seen in Figs. 6 and 7, the thermal degradation of microparticles was influenced by the surface roughness, the particle size and the salt content. Thus, the rate of degradation of samples with a high salt content (batch nos. 1, 3 and 6) was slightly lower than those with a low salt content (batch nos. 2, 4 and 5).

3.5. Characteristics of absorbing and releasing heat energy by the microparticles

The salt hydrates have not been investigated as heat storage materials to the same extent as the organic phase change materials. These materials present some disadvantages due to their instability, following dehydration in the process of thermal cycling and

Table 3
Results of thermogravimetric analysis.

Sample	Step I		Step II		Step III		Step IV	
	Temperature range	Mass losses (%)	Temperature range	Mass losses (%)	Temperature range	Mass losses (%)	Temperature range	Mass losses (%)
DSP	30–246	59.3	246–345	3.3	–	–	–	–
CAB	250–370	86.4	370–520	13.6	–	–	–	–
Batch 1	100–240	0.5	240–320	10.2	320–428	10.7	428–600	2.1
Batch 2	100–220	1.3	220–315	9.6	315–420	25.2	420–600	2.8
Batch 3	100–203	10.3	203–315	2.6	315–420	8.2	420–600	2.0
Batch 4	100–200	0.0	200–320	26.6	320–390	38.2	390–600	11.4
Batch 5	100–225	15.7	225–320	15.2	320–420	21.1	420–600	5.3
Batch 6	100–200	0.5	200–322	13.8	322–375	4.6	375–600	3.5

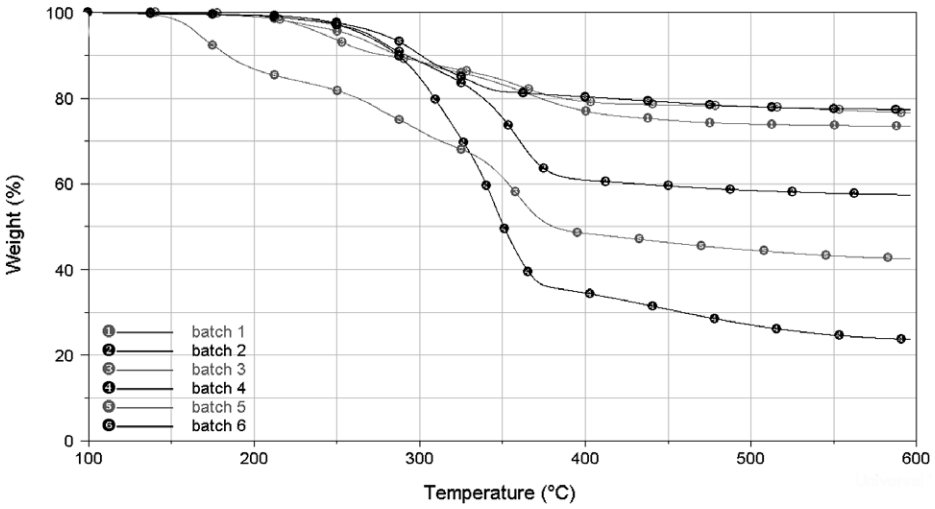

Fig. 6. TG curves of microparticles from batch nos. 1, 2, 3, 4, 5 and 6.

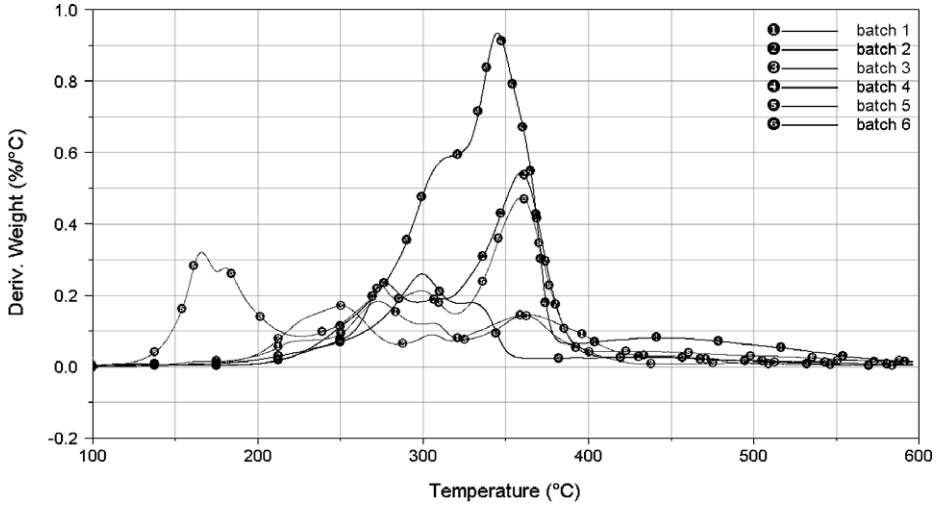

Fig. 7. DTG curves of microparticles from batch nos. 1, 2, 3, 4, 5 and 6.

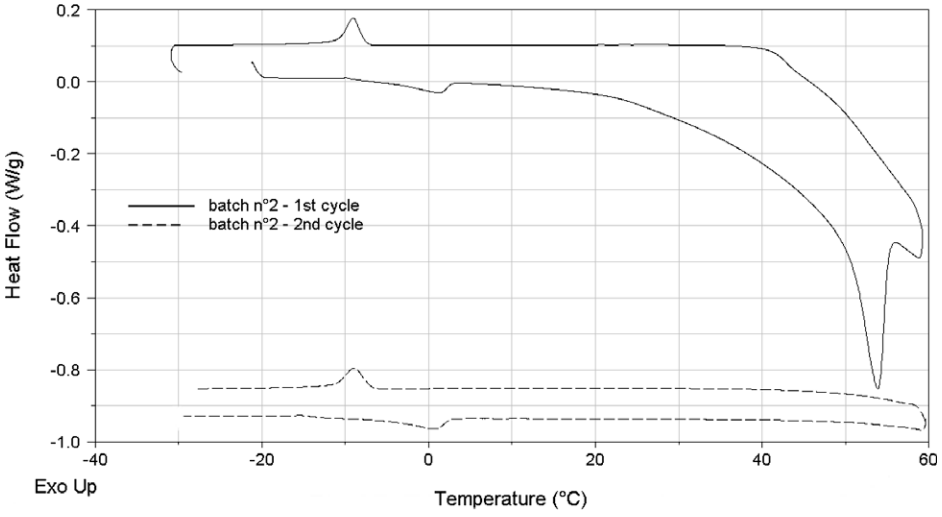

Fig. 8. DSC curves of microparticles from batch no. 2 (N_2, 2 °C/min).

a high degree of supercooling. The major instability of DSP is phase separation due to a semi congruent melting at 36 °C (Ryu, Woo, Shin, & Kim, 1992). Due to the porous morphology and the presence of no encapsulated salt in the batch no. 1, the DSC analysis was not performed. Fig. 8 displays the DSC curves of microparticles from batch no. 2 during two heating and cooling cycles. It can be seen that, the phase change temperature of the microparticles associated with a lower latent heat was very close to 0 °C. Furthermore, a wide endothermic peak was appeared in the first run of the DSC curves (from 20 to 60 °C), suggesting a melting process of a mixture of DSP/water associated with a loss of hydroscopic water molecules, e.g. a dehydration of the PCM (Table 4). When these microencapsulated PCM were subjected to a heating process for the second time, they could not be melted (2nd run in Fig. 8). Thus, they remained in an uncrystalizable state and can be rejected summarily for latent heat storage purposes. Fig. 9 shows the DSC curves of microparticles from batch nos. 3, 4 and 6. It can be seen that, the DSC curves present two endothermic peaks during the heating process (Table 4), and the absence of exothermic peak corresponding to the crystallization is also observed. Therefore, rehydration of the inorganic salts hydrates from the melting solution cannot be further proceeded. From the DSC curves of the Fig. 10, phase change temperatures for melting and freezing were determined as 26.69 and −0.50 °C for the microparticles from batch no. 5, suggesting that the thermal properties in a heating process of the microencapsulated PCM was similar to its core of DSP. The latent heat of fusion of these microencapsulated PCM was 140.4 J/g, less than 279 J/g of DSP due to the existence of the CAB/MDI shell.

Table 4
Thermal properties and peak assignments of microparticles synthesized in this study.

Sample	1st Peak		2nd Peak	
	T_m Onset (°C)	T_m Peak (°C)	T_m Onset (°C)	T_m Peak (°C)
Batch 2	−5.21	1.11	50.33	53.88
Batch 3	−5.57	1.05	56.28	79.83
Batch 4	−6.11	0.0	43.26	79.97
Batch 5	–	–	26.69	37.55
Batch 6	25.05	27.89	36.81	43.10

4. Conclusion

CAB/MDI microparticles containing an hydrated salt as phase change material were prepared by an interfacial polymerization.

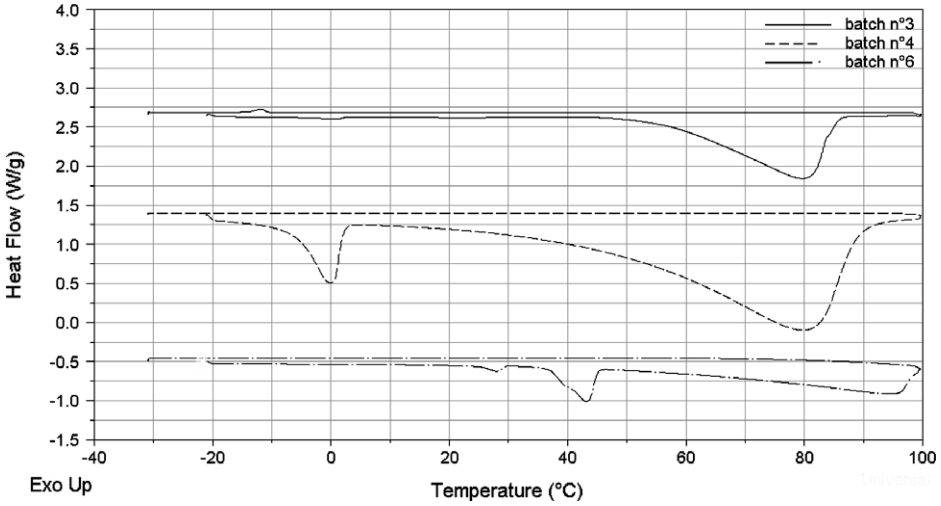

Fig. 9. DSC curves of microparticles from batch nos. 3, 4, and 6 (N_2, 2 °C/min).

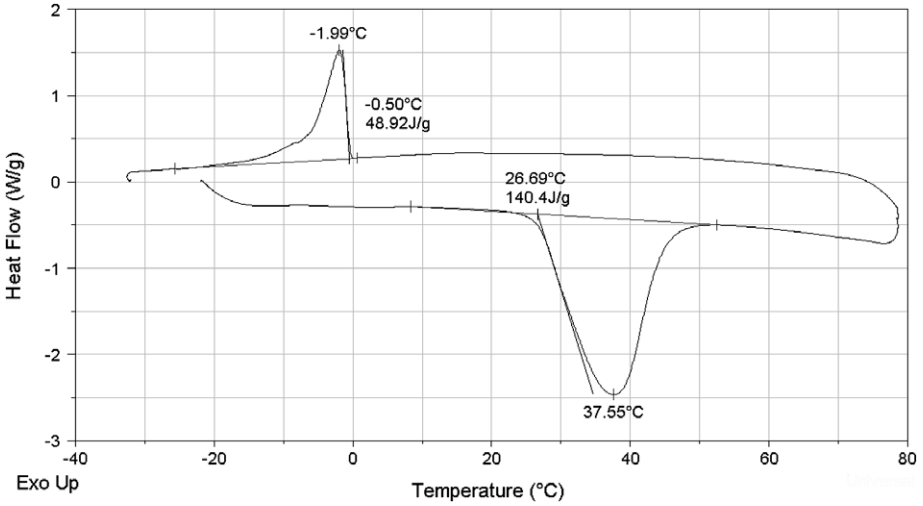

Fig. 10. DSC curves of microparticles from batch no. 5 (N_2, 2 °C/min).

The SEM analysis showed that the surface morphology is affected by many interrelated parameters, specially the nature of solvent used, and their boiling point. The SEM pictures show also that these microparticles are porous and spherical in shape. The surface appearance of microparticles depends on the rate of polymer precipitation at the interface. Thus, their surface is generally smooth when the polymer precipitates slowly due to slow removal of the organic solvent and a resulting porous morphology was obtained with a relatively faster precipitation of the polymer. Furthermore, better thermal stability at high temperature and the thermal degradation were strongly influenced by the loading content and the surface roughness. Microparticles from batch no. 5 were found most suitable for latent heat storage purposes on the basis of their stability in melting temperature and latent heat of fusion.

Appendix 1. Method of Hoy

The structural unit of CAB is

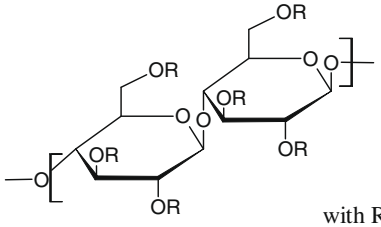

with R= H, OCH_3 or $OCH_2CH_2CH_3$

The method of Hoy is a group contribution method, thus for each chemical group in the molecule, contributions are added to the total. It contains four additive molar functions, a number of auxiliary equations and the final expressions for δ_d, δ_p and δ_h (Hoy, 1989).

Group	F_{ti} ($J^{1/2}$ $cm^{3/2}$ mol^{-1})	F_{pi} ($J^{1/2}$ $cm^{3/2}$ mol^{-1})	$\Delta T_i^{(P)}$	V_i (cm^3 mol^{-1})
5.5 $-CH_3-$	1669.25	0.0	0.121	118.525
8.8 $-CH_2-$	2367.2	0.0	0.176	136.84
10 –CH–	1760.0	0.0	0.13	95.6
0.5 –OH	337.5	242.5	0.0245	5.325
4 –O–	940.0	864.0	0.072	25.8
5.5 –COO–	3520.0	2904	0.22	130.35
2 Ring	−96.0	122.0	−0.007	–
Sum	10,497.95	4132.5	0.7365	512.44

F_{ti} is the molar attraction function, F_{pi} its polar component; V_i is the molar volume of structural unit of CAB. $\Delta T_i^{(P)}$ is the Lyderson correction for non-ideality, used in the auxiliary equations.

From the Hoy's method:

$$\delta_t = \frac{F_t + \frac{B}{\bar{n}}}{V}$$

where B, the base volume, is equal to 277, and $\bar{n}$ is given by the following auxiliary equation:

$$\bar{n} = \frac{0.5}{\Delta T^{(P)}} = \frac{0.5}{0.7365} = 0.6789$$

Therefore $\delta_t = 21.3\ \mathrm{MPa}^{\frac{1}{2}}$

$$\delta_P = \delta_t\left(\frac{1}{\alpha^{(P)}}\frac{F_P}{F_t + B/\bar{n}}\right) \quad \text{with } \alpha^{(P)} = \frac{777\Delta_T^{(P)}}{V} \quad \text{thus } \delta_P = 7.2\ \mathrm{MPa}^{\frac{1}{2}}$$

$$\delta_h = \delta_t\left(\frac{\alpha^{(p)} - 1}{\alpha^{(p)}}\right)^{\frac{1}{2}} = 6.9\ \mathrm{MPa}^{\frac{1}{2}}$$

$$\delta_d = (\delta_t^2 - \delta_p^2 - \delta_h^2)^{\frac{1}{2}} = 18.8\ \mathrm{MPa}^{\frac{1}{2}}$$

Appendix 2. Method of Krevelen and Hoftyzer

Addition of the group contribution gave:

Group	F_d ($J^{1/2}$ $cm^{3/2}$ mol^{-1})	F_p^2 ($J^{1/2}$ $cm^{3/2}$ mol^{-1})	Eh (J mol^{-1})
5.5 $-CH_3-$	2310	0.0	0.0
8.8 $-CH_2-$	2376	0.0	0.0
10 –CH–	800	0.0	0.0
0.5 –OH	105	62,500	10,000
4 –O–	400	2,560,000	12,000
5.5 –COO–	2145	7,263,025	38,500
2 Ring	380		
Sum	8516	9,885,525	60,500

$$\delta_d = \frac{\sum F_d}{V} = 16.6\ \mathrm{MPa}^{\frac{1}{2}}$$

$$\delta_p = \frac{(\sum F_p^2)^{\frac{1}{2}}}{V} = 6.1\ \mathrm{MPa}^{\frac{1}{2}}$$

$$\delta_h = \left(\frac{\sum Eh}{V}\right)^{\frac{1}{2}} = 10.9\ \mathrm{MPa}^{\frac{1}{2}}$$

Appendix 3. Results and average

The results of the two methods for estimation of the Hansen parameters are of the same order of accuracy, the average results were taken.

	Hoy	Krevelen–Hoftyser	Average
δ_d ($MPa^{\frac{1}{2}}$)	18.8	16.6	17.7
δ_p ($MPa^{\frac{1}{2}}$)	7.2	6.1	6.6
δ_h ($MPa^{\frac{1}{2}}$)	6.9	10.9	8.9

References

Arshady, R. (1990). Microspheres and microcapsules, a survey of manufacturing techniques: Part III: Solvent evaporation. *Polymer Engineering and Science, 30*(15), 915–924.

Cho, J., Kwon, A., & Cho, C. (2002). Microencapsulation of octadecane as a phase-change material by interfacial polymerization in an emulsion system. *Colloid & Polymer Science, 280*, 260–266.

Colvin, D. P., & Bryant, Y. (1988). Fibre with reversible enhanced thermal storage properties and fabric made there from. *US Patent Office*, Pat. No. 4 756 958.

El Bahri, Z., & Taverdet, J.-L. (2007). Elaboration and characterisation of microparticles loaded by pesticide model. *Powder Technology, 172*(1), 30–40.

Erkan, G., & Sariisik, M. (2004). Microencapsulation in textiles. *Colourage, 51*, 61–64.

Fan, Y. f., Zhang, X. X., Wang, X. C., Li, J., & Zhu, Q. B. (2004). Super-cooling prevention of microencapsulated phase change material. *Thermochimca Acta, 413*, 1–6.

Freitas, S., Merkle, H. P., & Gander, B. (2005). Microencapsulation by solvent extraction/evaporation: Reviewing the state of the art of microsphere preparation process technology. *Journal of Controlled Release, 102*(2), 313–332.

Fundueanu, G., Constantin, M., Esposito, E., Cortesi, R., Nastruzzi, C., & Menegatti, E. (2005). Cellulose acetate butyrate microcapsules containing dextran ion-exchange resins as self-propelled drug release system. *Biomaterials, 26*(20), 4337–4347.

Ghule, A., Bhonghale, C., & Chang, H. (2003). Monitoring dehydration and condensation processes of $Na_2HPO_4{\cdot}12H_2O$ using thermo-Raman spectroscopy. *Spectrochimica Acta Part A, 59*, 1529–1539.

Hansen, C. M. (1967). The three dimensional solubility parameter – key to paint component affinities: II and III. *Journal of Paint Technology, 39*(511), 505–514.

Hansen, C. M. (1969). The universality of the solubility parameter concept. *Industrial and Engineering Chemical Product Research and Development, 8*, 2–11.

Hirano, S., & Saitoh, T. S. (2002). Growth rate of crystallization in disodium hydrogenphosphate dodecahydrate. *Journal of Thermophysics and Heat Transfer, 16*(1), 135–140.

Hirano, S., Saitoh, T. S., Oya, M., & Yamazaki, M. (2001). Temperature dependence of thermophysical properties of disodium hydrogenphosphate dodecahydrate. *Journal of Thermophysics and Heat Transfer, 15*(3), 340–346.

Hoy, K. L. (1989). Solubility parameter as a design parameter for water borne polymers and coatings. *Journal of Coated Fabrics, 19*, 53–67.
Kistmundsdottir, T., & Ingvarsdottir, K. (1994). Influence of emulsifying agents on the properties of cellulose acetate butyrate and ethylcellulose microcapsules. *Journal of Microencapsulation, 11*(6), 633–639.
Laskar, J., Vidal, F., Fichet, O., Gauthier, C., & Teyssié, D. (2004). Synthesis and characterization of interpenetrating networks from polycarbonate and cellulose acetate butyrate. *Polymer, 45*(15), 5047–5055.
Leitch, P., & Tassinari, T. H. (2000). New materials in the new millennium. *Journal of Industrial Textiles, 29*(3), 173–191.
Mana, Z., Pellequer, Y., & Lamprecht, A. (2007). Oil-in-oil microencapsulation technique with an external perfluorohexane phase. *International Journal of Pharmaceutics, 338*(1–2), 231–237.
Moldenhauer, M. G., & Nairn, J. G. (1992). The control of ethylcellulose microencapsulation using solubility parameters. *Journal of Controlled Release, 22*(33), 205–218.
Mondal, S. (2008). Pase change materials for smart textiles – An overview. *Applied Thermal Engineering, 28*, 1539–1550.
Nelson, G. (1991). Microencapsulates in textile coloration and finishing. *Review of Progress in Coloration and Related Topics, 21*, 72–85.
Nelson, G. (2002). Application of microencapsulation in textiles. *International Journal of Pharmaceutics, 242*(1-2), 55–62.
Pause, B. (1995). Development of heat and cold insulating membrane structures with phase change material. *Journal of Coated Fabric, 25*(7), 59–68.
Ryu, H. W., Woo, S. W., Shin, B. C., & Kim, S. D. (1992). Prevention of supercooling and stabilization of inorganic salt hydrates as latent heat storage materials. *Solar Energy Materials and Solar Cells, 27*, 161–172.
Salaün, F., Devaux, E., Bourbigot, S., & Rumeau, P. (2008). Development of a precipitation method intended for the entrapment of hydrated salt. *Carbohydrate Polymer, 73*(2), 231–240.
Sarier, N., & Onder, E. (2007). The manufacture of microencapsulated phase change materials suitable for the design of thermally enhanced fabrics. *Thermochimica Acta, 452*(2), 149–160.
Talvenmaa, P., & Meinander, H. (2007). Possibilities of inorganic phase change materials to regulate body temperature in hot and cold environment. *Proceedings of intelligent textiles and mass customisation international conference* (pp. 336–345).
Tianyong, Z., Xuening, F., Jian, S., & Chunlong, Z. (1999). Properties of copper phthalocyanine microencapsulated in polystyrene by phase separation. *Dyes and Pigments, 44*(1), 1–7.
Torres, D., Boado, L., Blanco, D., & Vila-Jato, J. L. (1998). Comparison between aqueous and non-aqueous solvent evaporation methods for microencapsulation of drug–resin complexes. *International Journal of Pharmaceutics, 173*(1–2), 171–182.
Uda, K., & Hijikigawa, M. (1988). Moisture sensor containing cellulose acetate butyrate. *US Patent Office*, Pat. No. 4 773 935.
van Krevelen, D. W., & Hoftyzer, P. J. (1990). *Properties of polymers: Their estimation and correlation with chemical structure*. Amsterdam: Elsevier.
Zhang, X., Tao, X., Yick, K., & Wang, X. (2004). Structure and thermal stability of microencapsulated phase-change materials. *Colloid & Polymer Science, 282*, 330–336.